

## ELECTRONIC STRUCTURE AND OPTICAL PROPERTIES OF CUBIC $\text{NaNbO}_3$ AND TETRAGONAL $\text{KNbO}_3$ CRYSTALS: FIRST PRINCIPLES STUDY

S. AZAM<sup>a\*</sup>, M. IRFAN<sup>b</sup>, Z. ABBAS<sup>b</sup>, M. RANI<sup>c</sup>, T. SALEEM<sup>c,d</sup>, A. YOUNUS<sup>e</sup>,  
N. AKHTAR<sup>c</sup>, B. LIAQAT<sup>c</sup>, M. SHABBIR<sup>f,h</sup>, ABDULLAH G. AL-SEHEMI<sup>g,h</sup>

<sup>a</sup>*Faculty of Engineering and Applied Sciences, Department of Physics, RIPHAH International University, Islamabad, Pakistan*

<sup>b</sup>*Department of Physics, The University of Lahore, Sargodha Campus 40100, Pakistan*

<sup>c</sup>*Department of Physics The Women University Multan, Pakistan.*

<sup>d</sup>*Bahauddin Zikariya University Multan*

<sup>e</sup>*Laser matter interaction and nanosciences lab, department of physics. University of agriculture Faisalabad, Pakistan*

<sup>f</sup>*Department of Physics, College of Science, King Khalid University, Abha, 61413, P.O. Box 9004, Saudi Arabia*

<sup>g</sup>*Department of Chemistry, College of Science, King Khalid University, Abha, 61413, P.O. Box 9004, Saudi Arabia*

<sup>h</sup>*Research Center for Advanced Materials Science (RCAMS), King Khalid University, P.O. box 9004, Abha 61413, Saudi Arabia*

Cubic sodium niobate ( $\text{NaNbO}_3$ ) and tetragonal potassium niobate ( $\text{KNbO}_3$ ) crystals are studied using the Wien2k code. Lattice parameters are optimized by using generalized gradient approximations and results compared with existing experimental data. Electronic properties such as total and partial density of states (TDOS and PDOS), band structures have been calculated for both cubic and tetragonal phase of sodium and potassium niobate  $\text{NaNbO}_3$  and  $\text{KNbO}_3$  crystals, respectively. The indirect band gaps are observed for both phases. The electronic and optical properties of  $\text{NaNbO}_3$  and  $\text{KNbO}_3$  crystals are calculated by first principles using (GGA+U) approximations for both cubic and tetragonal phase. For both phases, the real and imaginary parts of complex dielectric function and thus optical constants such as absorption coefficient, energy loss function, reflectivity, refractive index, extinction coefficients and optical conductivity are calculated. The computed optical spectra of cubic and orthorhombic phases are compared with the experimental data and found good agreement with the results.

(Received April 10, 2019; Accepted August 30, 2019)

**Keywords:** Electronic structure, Optical properties, Wien2k, DFT

### 1. Introduction

Perovskite belongs to a class of Ferroelectric materials with the chemical formula of  $\text{ABO}_3$ . Where A is a cation which could be monovalent or divalent, whereas B is a pentavalent or tetra valent metal [1]. The perovskite structure materials have very interesting properties like; they can easily undergo phase transitions. The transitions are of different variety like transition to ferroelectric and anti-ferroelectric and insulator metal transitions. They show superconductive behavior and piezoelectric anisotropy. The perfect perovskite structure has cubic symmetry in which A and B cations are attached with oxygen. The oxygen ions are sharing corners with B cation at the center on the lattice. While A cation lies between the octahedra at 12-fold coordinated sites. This structure shows large range of structural instabilities which involves distortions or

---

\*Corresponding author: sikander.physicst@gmail.com

rotation of oxygen ion and cation displacement from their sites. Photocatalytic activity is high as the energy band gap is in visible region [2-4].

Sodium and potassium niobate  $\text{NaNbO}_3$  and  $\text{KNbO}_3$  crystals are most investigated materials in the famous class of perovskite structure ferroelectrics. As their important technological applications, both materials have been subjected to several first principles calculations. Among these perovskite, piezoelectric lead free ceramic materials have become very famous because of their environmental protection point of view.  $\text{ANbO}_3$  ( $A=\text{Na, Li and K}$ ) are studied as piezoelectric lead-free candidate [5]. Under atmospheric pressure in stabilized phases, at high temperature 1210 °C, only structural phase transition is exhibited by  $\text{LiNbO}_3$ . But sodium niobate  $\text{NaNbO}_3$  and potassium niobate  $\text{KNbO}_3$  shows different structural phase transitions [6].  $\text{NaNbO}_3$  has very complex transition process and shows several polymorphs under different temperatures. Due to uses in  $\text{CO}_2$  reduction and generating hydrogen, photocatalytic properties of  $\text{NaNbO}_3$  are of much focus. However, the use of sunlight is limited by bad optical absorption due to band gap of 3.49eV [7]. Visible light and piezoelectric properties can be increased by doping [8]. Among other candidates for piezoelectric lead free ceramics, most promising is potassium sodium niobate  $\text{KNbO}_3$ , because of improved environmental compatibility, good piezoelectric and ferroelectric properties [9]. Zhou et al. studied electronic, optical and structural properties of  $\text{NaNbO}_3$ ,  $\text{KNbO}_3$  and  $\text{K}_{0.5}\text{Na}_{0.5}\text{Nb}_{0.3}$  using DFT plane-wave pseudo-potential method. Studies of electronic structure revealed lower conduction bands and similar valence bands of all three compound. Likewise optical properties explored that at low energies optical spectrum is mainly due to valence band transition O-2p to conduction band Nb-4d. While optical spectrum at high energies is mainly due to the transitions at K-4s4p or Na-3s3p states. Their conclusion revealed that the properties of KNN can be changed by altering the Na/K ratio at high energy region. [10]. Fritsch studied  $\text{NaNbO}_3$  for different crystalline phases using density functional theory. They explored optical, electronic and structural properties. The calculations were performed at room temperature and below room temperature. Their conclusions include better performance of improved GGA functional AM05 and PBEsol in comparison with conventional PBE. The findings of this research are in good agreement with experimental results [11, 12].

In this manuscript, we have made first principles DFT calculations based on full potential linearized augmented plane wave method (FP-LAPW) is implemented in Wien 2k, computations for the optoelectronic and structural properties of  $\text{NaNbO}_3$  and  $\text{KNO}_3$  materials for both phases. Some comparisons with other related theoretical and experimental work is made where it is necessary.

## 2. Computational detail

Present calculations have been performed with simulations package Wien-2k. Full potential augmented plane wave (FP-LAPW) method is used for the description of valence electrons and ionic cores. The exchange correlations potentials generalized gradient plus Hubbard parameter (GGA+U) approximations are used for the description of electron-electron interactions. The valence states for the computations are  $1s^2 2s^2 2p^6 3s^1$  for Na,  $3s^2 3p^6 4s^1$  for K,  $4p^6 4d^4 5s^1$  for Nb and  $2s^2 2p^4$  for O. The convergence of DFT calculations is obtained by using Monkhorst pack k points grid  $7 \times 7 \times 7$ , plane wave cut of energy 500 eV and sigma 0.2 for both the  $\text{NaNbO}_3$  and  $\text{KNbO}_3$  crystals. The self consistent iterations are attained until the accuracy of convergence reaches  $10^{-6}$  eV. The ionic positions and cell parameters are relaxed to gain the equilibrium geometry for  $\text{NaNbO}_3$  and  $\text{KNbO}_3$  crystals using GGA+U method and the optimized parameters are used for the calculations of electronic structure. The optical properties are calculated from the complex dielectric function  $\varepsilon(\omega) = \varepsilon_1(\omega) + i\varepsilon_2(\omega)$ . The real and imaginary parts were calculated Kramers-Kronig relation (KKR) and momentum matrix elements respectively. Furthermore, the calculated bandgaps with local density and generalized gradient approximations are usually underestimated, so we used GGA+U approximation for accuracy. Consequently, Wien 2k method is employed for improvement of optoelectronic and structural properties of observed crystals.

### 3. Results and discussion

#### 3.1. Structure characteristics

In this work cubic and tetragonal phases of  $\text{NaNbO}_3$  and  $\text{KNbO}_3$  crystals respectively under studied. Both of materials sodium and potassium niobate have perovskite structure having space groups  $\text{Pm}\bar{3}\text{m}$  (221) and  $\text{P4mm}$  (99) respectively. The calculations are carried out by the origin of the cell to be at Na site (0,0,0), Nb at the body-centre (0.5, 0.5, 0.5)a and the three O atoms at the three face centers (0.5, 0.5, 0.0)a, (0.0, 0.5, 0.5)a and (0.5, 0.0, 0.5)a. The calculation are performed by experimental data for lattice constants  $a = b = c = 7.86 \text{ \AA}$  in the cubic phase. For the tetragonal phase K(0.5,0.5,0.5), Nb(0,0,0.02) and O atoms at (0.5,0,0.97)a, (0,0.5,0.97)a and (0,0,0.46)a sites of  $\text{KNbO}_3$  are placed. We used the crystallographic data with lattice constant of  $a = b = 7.90 \text{ \AA}$  and  $c = 8.27 \text{ \AA}$ . For the study of structural properties of these crystals, the total energies for different volumes are calculated and then fitted to Murnaghan's equation of states, to find the bulk modulus ( $B_0$ ), pressure derivatives ( $B'$ ) and lattice constants ( $a_0$ ). For the cubic phase of  $\text{NaNbO}_3$ , the calculated lattice parameters theatrically are observed by minimizing the ratio of energy of crystal to volume. The comparison in present theoretical and previous is shown in Table 1. The accuracy of these results lies in the range of local density approximations. So, our results for cubic phase of  $\text{NaNbO}_3$  by first principles calculations suggest that our FP-LAPW is reliable and the work is better. Consequently, the calculated equilibrium parameters are quite in good agreement with experimental data by GGA+U approximations. The relaxed structure of tetragonal  $\text{KNbO}_3$  is calculated after optimization of a and c.

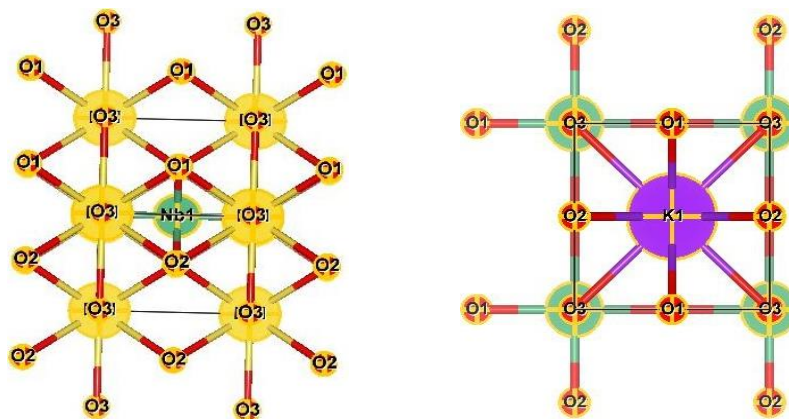


Fig. 1. Crystal structures for cubic  $\text{NaNbO}_3$  and tetragonal  $\text{KNbO}_3$ .

Table 1. Computed equilibrium bulk modulus  $B_0$  (in GPa), and the pressure derivative of the bulk modulus  $B'$ .

Crystals	$B_0$	$B'$
$\text{NaNbO}_3$	183.18	4.60
$\text{KNbO}_3$	100.0 198.23[32]	5.0 4.78[32]

#### 3.2. Band structure

The band structure (BS) and density of states (DOS) for cubic and tetragonal phase of  $\text{NaNbO}_3$  and  $\text{KNbO}_3$ , respectively is plotted with high symmetry of Brillouin zone (BZ) axes as shown in figure 2 and 3. The origin of energy is set up at valence band maximum (VBM), and is taken in electron volt. The high symmetry BZ points of cubic sodium niobate consists of:  $\text{R}(1/2,1/2,1/2)$ ,  $\Gamma(0,0,0)$ ;  $\text{X}(0,1/2,0)$ ;  $\text{M}(1/2,1/2,0)$ ; and for tetragonal potassium niobate  $\text{R}(0,1/2,1/2)$ ,  $\Gamma(0,0,0)$ ;  $\text{X}(0,1/2,0)$ ;  $\text{M}(1/2,1/2,0)$ ; The band gap, the electronic structure of VB and low energy conduction band are the significant properties in applications of electronic devices.

The valence band normally formed below Fermi level due to O(s/p), Nb(s/p/d) and Na(p) and K(p) states NaNbO<sub>3</sub>, KNbO<sub>3</sub> for cubic and tetragonal structure respectively. The bottom band for cubic structure lies between -5.5 eV and -3 eV formed due to O(s) orbitals. Near Fermi level nine valence bands are formed due to O(p) orbitals between 0.0 to -5 eV. The valence band maximum lies on high symmetry point (M) and conduction band lies on (Γ) point indicates indirect band gap for both spin up and down polarizations for NaNbO<sub>3</sub>. Our computed value of indirect band gap for the cubic structure of NaNbO<sub>3</sub> crystal is 1.8 eV. For tetragonal structure of KNbO<sub>3</sub>, the observed band gap is also indirect due to different symmetries points of VBM and CBM. The calculated indirect bandgap is 1.4 eV for tetragonal structure. In cubic structure of sodium niobate (NaNbO<sub>3</sub>) crystal, nine valence bands at gamma point having three triply degenerate levels. The splitting is produced due to electrostatic interactions and crystal field between O (p) orbitals.

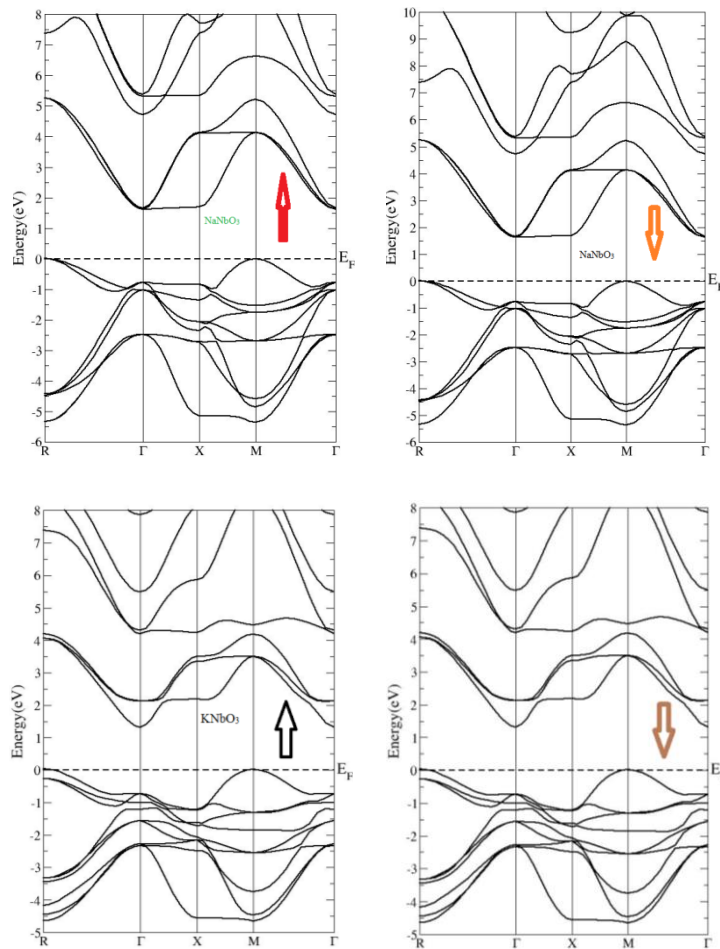


Fig. 2. (a-d). Electronic band structures of cubic NaNbO<sub>3</sub> and tetragonal KNbO<sub>3</sub>.

For further clarifications of bands/elements role in electronic band structure, total and partial densities of states (TDOS, PDOS) are calculated for cubic NaNbO<sub>3</sub> and KNbO<sub>3</sub>. The calculated TDOS is shown in Fig. 3, reveals a clear difference in bands between cubic and tetragonal structures respectively for both spin up and down. The TDOS for both cubic and tetragonal phase of crystals are same due to polarizations, which show small effect on the band structure of materials. The PDOS diagram shows the valence conduction bands are mainly formed due to hybridizations O(p), Nb(d) and Na(s) states for NaNbO<sub>3</sub> and has minute effect of O(s), Nb(s,p) and Na(p) states shown in Fig. 4a. For KNbO<sub>3</sub> crystal, valence and conduction band mainly generated due to hybridization of O(p), Nb(p,d) and K(p) states and O(s), Nb(s) and K(s) states contribute minutely as observed in Fig. 4b. At centre of Brillouin zone significant dispersion

occur for the conduction band states, which are manifested by high electron mobility. The shapes of VBs are flat in the X-M direction showing low hole mobility.

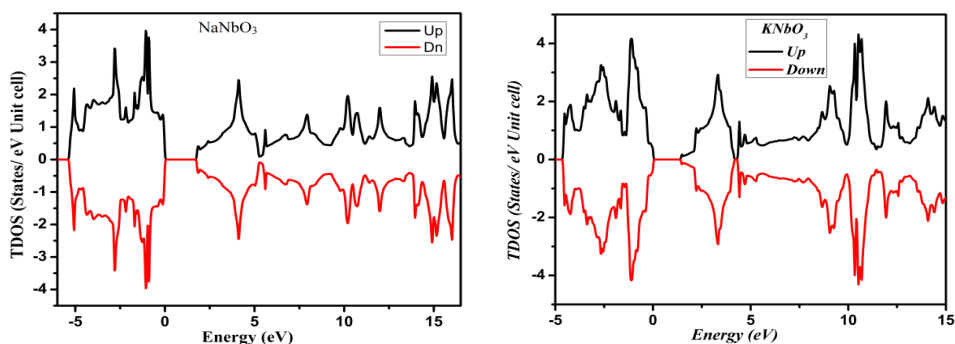


Fig. 3. TDOS for cubic  $\text{NaNbO}_3$  and tetragonal  $\text{KNbO}_3$  crystals.

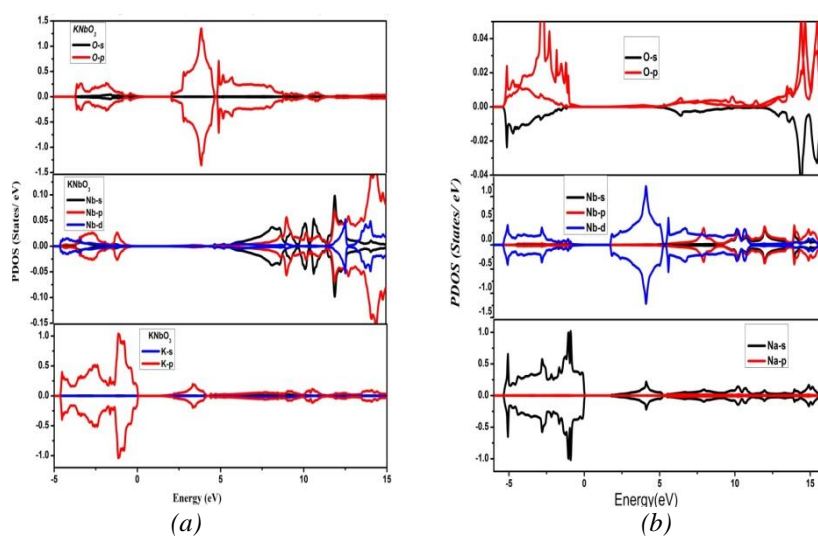


Fig. 4. PDOS for (a) cubic  $\text{NaNbO}_3$  and (b) tetragonal  $\text{KNbO}_3$  crystals.

The bandgaps are calculated using GGA+U approximations and the results are available for comparison of experimental data [13-20] in table 2. In present study GGA+U calculations are performed and computed bandgaps exhibits indirect nature. The experimental bandgap lies in 3.10-3.95 and 3.42-3.76 eV for  $\text{NaNbO}_3$  and  $\text{KNbO}_3$ , respectively. Consequently, our obtained bandgaps for both cubic and tetragonal structure materials are reduced on comparing other theoretical and experimental data. The probable cause is illustrated as: Firstly, the bandgaps calculated with GW are considered as fundamental bandgaps. Though, the experimental results were calculated from optical spectra which have electron-hole interaction s( excitonic effect) and more screening of quasiparticle excitation owing to electron-hole coupling(polaronic effect)[21], which may reduce the bandgap of the materials. Secondly, the accuracy of our theoretical results depends on computational cost and related parameters sets which also manipulate the calculations reliability. Furthermore, different experiment techniques can also influence the bandgaps of the compounds.

Table 2. Comparison of theoretical and experimental band gap (in eV) of NaNbO<sub>3</sub> and KNbO<sub>3</sub> structure.

	Cubic NaNbO <sub>3</sub>	Tetragonal KNbO <sub>3</sub>
Band gap (this work)(indirect)	1.8 3.42[25] 3.2[26]	1.4 1.40[21] 1.58[22]
Experimental	3.10[27]	1.43[23] 3.30[24]

### 3.3. Optical properties

The optical properties for the NaNbO<sub>3</sub> and KNbO<sub>3</sub> are obtained by frequency dependent dielectric function are computed by summing conduction band states on limit of long wavelength (q=0). The imaginary part of dielectric function is calculated by 3×3 Cartesian tensor  $\epsilon_{\alpha\beta}$  is given as [28,29].

$$\epsilon_2(\omega) = \epsilon_{\alpha\beta}^{(2)} = \frac{4\pi^2 e^2}{\Omega} \lim_{q \rightarrow 0} \frac{1}{q^2} \times \sum_{c,v,k} 2\omega_k \delta(\epsilon_{ck} - \epsilon_{vk} - \omega) \times \langle u_{ck+e_{\alpha}q} | u_{vk} \rangle \langle u_{ck+e_{\beta}q} | u_{vk} \rangle^* \quad (1)$$

Here, v and c represents valence and conduction band states respectively, k refers reciprocal lattice vector and  $\omega$  is incident photon frequency.  $\Omega$  Indicates primitive cell volume and 2 factor is here before weight due to degeneracy of spin orbit system. The vectors  $e_{\alpha}$  and  $e_{\beta}$  represents unit vectors in Cartesian directions.

The real part of complex dielectric function is calculated from the imaginary part by using Kramer's- Kroning relations.

$$\epsilon_1(\omega) = \epsilon_{\alpha\beta}^{(1)}(\omega) = 1 + \frac{2}{\pi} P \int_0^{\infty} \frac{\epsilon_2(\omega')\omega'}{\omega'^2 - \omega^2 + i\eta} d\omega' \quad (2)$$

where P and  $\eta$  represents principal value and complex shift respectively calculated by CSHIFT in the VASP code.

Other optical constants i.e absorption coefficient, electron energy loss function, reflectivity, refractive index, extinction coefficient and optical conductivity is also calculated in the light of real and imaginary parts of complex dielectric function [30,31]

$$I(\omega) = \sqrt{2}\omega \left[ \sqrt{\epsilon_1^2(\omega) + \epsilon_2^2(\omega)} - \epsilon_1(\omega) \right]^{1/2} \quad (3)$$

$$L(\omega) = \frac{\epsilon_2(\omega)}{\epsilon_1^2(\omega) + \epsilon_2^2(\omega)} \quad (4)$$

$$R(\omega) = |\epsilon(\omega) - 1| / |\epsilon(\omega) + 1|^2 \quad (5)$$

The index of refraction is given by

$$\vec{n}(\omega) = n(\omega) + ik(\omega) \quad (6)$$

Real part represents refractive index while imaginary part is extinction coefficient. Refractive index is given by

$$n(\omega) = \frac{1}{\sqrt{2} \left[ \sqrt{\epsilon_1^2(\omega) + \epsilon_2^2(\omega)} + \epsilon_1(\omega) \right]^{1/2}} \quad (7)$$

$$k(\omega) = 1/\sqrt{2} \left[ \sqrt{\varepsilon_1^2(\omega) + \varepsilon_2^2(\omega)} - \varepsilon_1(\omega) \right]^{1/2} \quad (8)$$

The optical properties of cubic  $\text{NaNbO}_3$  and tetragonal  $\text{KNbO}_3$  will be discussed on the basis of above mentioned equations.

### 3.3.1. Dielectric function

The optical properties of cubic sodium niobate and tetragonal potassium niobate are calculated for both phases. The real and imaginary parts of complex dielectric function for both phases are shown in figure 5. They show smooth behaviour in the whole energy range 0-14 eV. Fig. 5a indicates static dielectric constant of real part are 3.3 and 2.8 for  $\text{NaNbO}_3$  and  $\text{KNbO}_3$  respectively. For  $\text{NaNbO}_3$  and  $\text{KNbO}_3$ , main peaks of real part  $\varepsilon_1(\omega)$  curves are 5.8 and 5 at energy 2 and 3 eV respectively, and for imaginary part  $\varepsilon_2(\omega)$  are 4 and 5.5 at 4.8 and 3.8 eV, correspondingly. At negative value of  $\varepsilon_1(\omega)$ , group velocity will be greater than speed of light exhibiting nonlinear response. Hence, the materials fall into superluminal region at high energy where both permittivity and permeability are negative. Imaginary part is most significant to characterize optical properties of the materials. Both the materials show isotropic nature up to 2 eV, which is due to bandgap of the materials. The first absorption edge starts at 1.7 and 1.9 eV for  $\text{NaNbO}_3$  and  $\text{KNbO}_3$  respectively, responsible for the direct transitions between valence and conduction bands at the  $\Gamma$  point. As imaginary part of dielectric function is related to transitions examined in the total and partial density of states. Figure 5b shows five major peaks 2.2, 4.0, 6.2, 8.0 and 12 eV for cubic structure of  $\text{NaNbO}_3$ . The peaks 2.2, 4.0 and 6.2 eV are formed with O (p)  $\rightarrow$  Nb (d- $t_{2g}$ ) transitions and other peaks 8.0 and 12 eV are related to O (p)  $\rightarrow$  Nb (d- $e_g$ ) transitions. For tetragonal phase of  $\text{KNbO}_3$  crystal, main peaks arise at 4.0, 5.7, 6.3, 9.2 and 11.1 eV, first three peaks are formed due to O (p)  $\rightarrow$  Nb (d- $t_{2g}$ ) and other two 9.2 and 11.1 eV are due to O(p)  $\rightarrow$  Nb (4d- $e_g$ ) transitions. Consequently, above analysis of main peaks in the absorption spectra plays critical role in the computations of optical properties of both crystals.

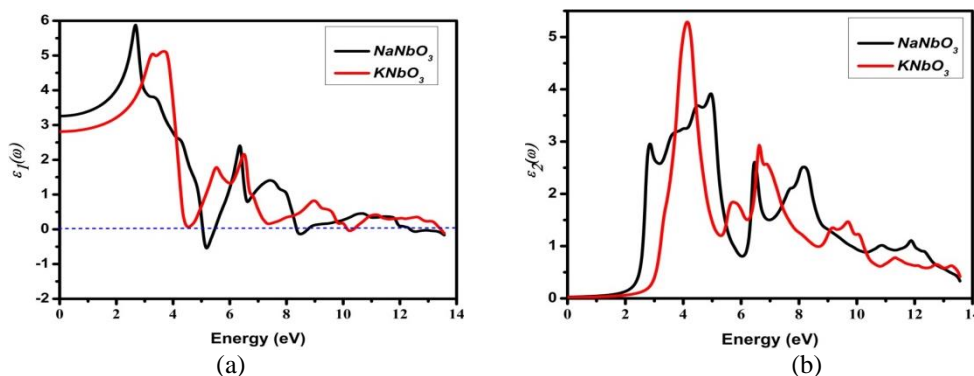


Fig. 5. Real and imaginary parts of (a) cubic  $\text{NaNbO}_3$  and (b) tetragonal  $\text{KNbO}_3$  crystals.

### 3.3.2. Electron energy-loss function, absorption function, reflective function, refractive function, and extinction coefficient

The energy loss function is related to loss of fast electrons traversing in the compounds is plotted for  $\text{NaNbO}_3$  and  $\text{KNbO}_3$  in Fig. 6b these peaks are formed due to binding electron oscillations and interband or intraband transitions. The maxima for  $\text{NaNbO}_3$  and  $\text{KNbO}_3$  lies around 12 eV for both crystals. The energy loss function is related of plasmonic oscillations and scattering probability of volume losses. The reflectivity spectra are indicated in figure 6c, shown peaks same as that of dielectric function and it varies widely with photon energy. This makes possible to the compounds suitable for optical applications.

The refractive index  $n(\omega)$  is related to dispersion of incident light and photons interactions with the crystals are plotted in figure 6d. When the value of refractive index lies between one and two, it is more effective in visible and ultraviolet region. As refractive index is alternative of real part of dielectric function and related with relation  $n_0^2 = \epsilon_1(0)$ . The value of  $n(\omega)$  starts increasing and reaches its peak value around 2.3 for cubic and tetragonal phase of crystals  $\text{NaNbO}_3$  and  $\text{KNbO}_3$  respectively. The extinction coefficient and imaginary part of complex dielectric function provide information about the absorption of light at band edges as shown in figure 6e.

The optical conductivity is expressed as  $\sigma(\omega) = \sigma_1(\omega) + \sigma_2(\omega)$ , is the sum of real and imaginary part of as shown in figure 6f for  $\text{NaNbO}_3$  and  $\text{KNbO}_3$ . The conductivity is calculated with dipole transitions in VBs and CBs. Upto 2 eV no peaks are found in plot, as this is linked with bandgap of the materials.  $\sigma(\omega)$  is also connected with frequency dependent of complex dielectric function as given  $\epsilon(\omega) = 1 + \frac{4\pi i \sigma(\omega)}{\omega}$ . The imaginary part of optical conductivity remains negative until at 5 and 6 eV and then approaches to positive as seen in figure. Optical transitions ( $\Gamma_v - \Gamma_c$ ) are responsible for real part of optical conductivity show six maxima.

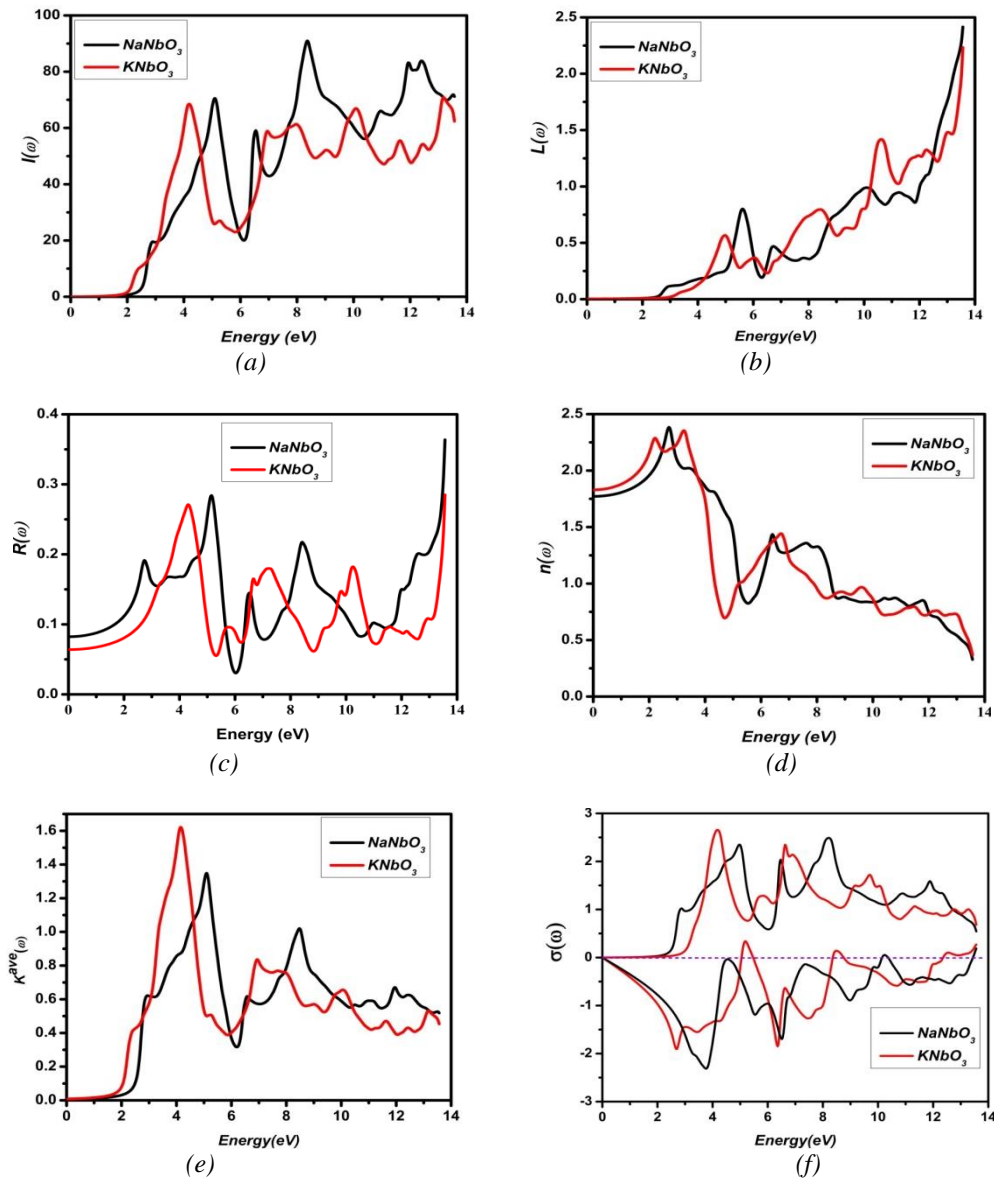


Fig. 6. Calculated optical spectra for  $\text{NaNbO}_3$  and  $\text{KNbO}_3$  crystals. (a) Absorption function (b) Energy-loss function (c) Reflectivity (d) Refractive index (e) Extinction coefficients (f) Optical conductivity.

#### 4. Conclusions

The study of structural, electronic and optical properties of cubic and tetragonal phase of  $\text{NaNbO}_3$ ,  $\text{KNbO}_3$  crystals respectively studied using first principled calculations. It is observed from band structure that both materials are small indirect bandgap semiconductors. The results of electronic properties of both cubic and tetragonal phase of crystals exhibit strong hybridization between O(s/p), Nb(s/p/d) and Na(p) and K(p) orbitals in  $\text{NaNbO}_3$ ,  $\text{KNbO}_3$ . The optical properties such as absorption coefficient, energy loss function, reflectivity, refractive index, extinction coefficients and optical conductivity are calculated by GGA+U approximations for both phases.

The spectral analysis indicate that strong absorption occur in the ultraviolet region mainly. So, both materials may be applied in the short wavelength optical devices as UV LEDs and UV detectors. For more effective applications as photocatalytic materials, large absorption must be lies in visible region which is greatest challenge. Further study for enhancement of optical properties is under considerations. The current work focus on the cubic and tetragonal phase of  $\text{NaNbO}_3$  and  $\text{KNbO}_3$  crystals respectively, more work on other phases for the investigation of properties is also under consideration.

#### Acknowledgement

The authors would like to acknowledge the support of King Khalid University for this research through a grant RCAMS/KKU/04-19 under the Research Center for Advanced Materials Science (RCAMS) at King Khalid University, Kingdom of Saudi Arabia.

#### References

- [1] M. E. Lines, A. Glass, Principles and Applications of Ferroelectric and Related Materials, Oxford Clarendon Press, (1977).
- [2] A. Shigemi, T. Wada, Mat. Res. Soc. Proc. **902E**, 0902-T10-46.1 (2006).
- [3] Xu, Yong-Qiang, Shao-Yi Wu, Li-Juan Zhang, Li-Na Wu, Chang-Chun Ding, Physica Status Solidi (b) **254**(5), 1600620 (2017).
- [4] K. Ueno, S. Nakamura, H. Shimotani, H. T. Yuan, N. Kimura, H. Aoki, Y. Iwasa, M. Kawasaki, Nature Nanotechnol. **6**, 408 (2011).
- [5] A. Mehta, A. Navrotsky, N. Kumadaand N. Kinomura, J. Solid State Chem. **102**, 213 (1993).
- [6] Y. Shiozaki, E. Nakamura and T. Mitsui: Landolt-Börnstein(Springer-Verlag, Berlin Heidelberg, New York, 2001) vol. III/36A1, p. 67.
- [7] H. Shi, T. Wang, J. Chen, et al., Catal. Lett. **141**, 525 (2011).
- [8] J. Yao, W. Ge, L. Yan, et al., J. Appl. Phys. **111**, 064109 (2012).
- [9] Y. Saito, H. Takao, T. Tani, T. Nonoyama, K. Takatori, T. Homma, T. Nagaya, M. Nakamura, Nature **432**, 84 (2004).
- [10] Fritsch, Daniel, Advances in Materials Science and Engineering 2018 (2018).
- [11] Yang, Dong, Qizhen Chai, Lingling Wei, Xiaolian Chao, Zupei Yang. Physical Chemistry Chemical Physics **19**(40), 27368 (2017).
- [12] Cabuk, Suleyman, Optoelectron. Adv. Mat. **1**(3), 100 (2007).
- [13] M. Tyunina, L. Yao, D. Chvostova, A. Dejneka, T. Kocourek, M. Jelinek, V. Trepakov, S. V. Dijken, Sci. Technol. Adv. Mater. **16**, 026002 (2015).
- [14] T. T. Zhang, K. Zhao, J. G. Yu, J. Jin, Y. Qi, H. Q. Li, X. J. Hou, G. Liu, Nanoscale **5**, 8375 (2013).
- [15] G. E. Jellison, Jr., I. Paulauskas, L. A. Boatner, and D. J. Singh, Phys. Rev. B **74**, 155130 (2006).
- [16] J. W. Liu, G. Chen, Z. H. Li, Z. G. Zhang, Int. J. Hydrogen Energy **32**, 2269 (2007)
- [17] H. Kato and A. Kudo, J. Phys. Chem. B **105**, 4285 (2001).
- [18] M. Wiegel, M. H. J. Emond, E. R. Stobbe, G. Blass, J. Phys. Chem. Solids **55**, 773 (1994).
- [19] K. Teramura, S. Okuoka, H. Tsuneoka, T. Shishido, T. Tanaka, Appl. Catal. B **96**, 565

- (2010).
- [20] H. W. Eng, P. W. Barnes, B. M. Auer, P. M. Woodward, *J. Solid State Chem.* **175**, 94 (2003).
  - [21] T. Neumann, G. Borstel, Scharfschwerdt, M. Neumann, *Phys. Rev. B.* **46**, 10623 (1992).
  - [22] C. M. I. Okoye, *J. Phys: Condens. Matter* **15**, 5945 (2003).
  - [23] E. E. Krasovskii, O. V. Krasovska, W. Schattke, *J. Electron Spectrosc. Relat. Phenom* **83**, 12 (1997).
  - [24] E. Wiesendanger, *Ferroelectrics* **6**, 263 (1974).
  - [25] P. Li, H. Abe, J. Ye, *Int. J. of Photoenergy* 1155 (2014).
  - [26] B. Modak, P. Modak, S. K. Ghosh, *RSC Adv.* 90188 (2016).
  - [27] J. Xu, B. Feng, Y. Wang, Y. Qi, J. Niu, M. Chen, *Front.*
  - [28] H. Wang, F. Wu, H. Jiang, *J. Phys. Chem. C* **115**, 16180 (2011).
  - [29] M. Gaidos, K. Hummer, G. Kresse, *Phys. Rev. B* **73**, 045112 (2006).
  - [30] J. Jalilian, M. Safari, S. Naderizadeh, *Comput. Mater. Sci.* **117**, 120 (2016).
  - [31] J. Sun, H. T. Wang, J. He, Y. J. Tian, *Phys. Rev. B* **17**, 125132 (2005).
  - [32] C. M. I. Okoye, *J. Phys.: Condens. Matter* 15, 5945 (2003).